THE JOURNAL OF PHYSICAL CHEMISTRY A

Article

pubs.acs.org/JPCA

Ru(II) Dyads Derived from 2-(1-Pyrenyl)-1*H*-imidazo[4,5-*f*][1,10]phenanthroline: Versatile Photosensitizers for Photodynamic Applications

Mat Stephenson,[†] Christian Reichardt,[‡,§] Mitch Pinto,[†] Maria Wächtler,[‡,§] Tariq Sainuddin,[†] Ge Shi,[†] Huimin Yin,[†] Susan Monro,[†] Eric Sampson,[†] Benjamin Dietzek,*[,‡,§] and Sherri A. McFarland*[,†]

[†]Department of Chemistry, Acadia University, Wolfville, NS B4P 2R6, Canada

[‡]Institute of Physical Chemistry and Abbe Center of Photonics, Friedrich-Schiller-University Jena, Helmholtzweg 4, 07743 Jena, Germany

[§]Leibniz Institute of Photonic Technology (IPHT), Albert-Einstein-Straße 9, 07745 Jena, Germany

Supporting Information

ABSTRACT: Combining the best attributes of organic photosensitizers with those of coordination complexes is an elegant way to achieve prolonged excited state lifetimes in Ru(II) dyads. Not only do their reduced radiative and nonradiative rates provide ample time for photosensitization of reactive oxygen species at low oxygen tension but they also harness the unique properties of ^{3}IL states that can act as discrete units or in concert with ^{3}MLCT states. The imidazo[4,5-*f*][1,10]phenanthroline framework provides a convenient tether for linking π-expansive ligands such as pyrene to a Ru(II) scaffold, and the stabilizing coligands can fine-tune the chemical and biological properties of these bichromophoric systems. The resulting dyads described in this study exhibited nanomolar light cytotoxicities against cancer cells with photocytotoxicity indices exceeding 400 for some coligands employed. This potency extended to bacteria, where concentrations as low as 10 nM destroyed 75% of a bacterial population. Notably, these dyads remained extremely active against biofilm with light photocytotoxicities against these more resistant bacterial populations in the 10−100 nM regime. The results from this study demonstrate the versatility of these highly potent photosensitizers in destroying both cancer and bacterial cells and expand the scope of compounds that utilize low-lying ^{3}IL states for photobiological applications.

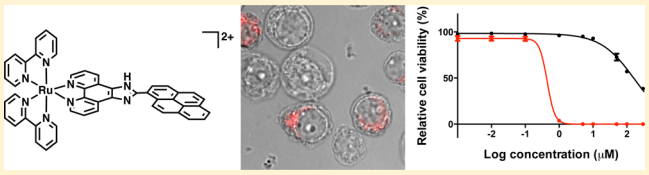

1. INTRODUCTION

Photosensitizers (PSs) as therapeutic agents and diagnostic tools afford the unique opportunity to use light as an external trigger to generate both temporal and spatial selectivity in applications from the photodynamic therapy (PDT) of cancer and age-related macular degeneration to photodynamic inactivation (PDI) of microorganisms. Minimization of collateral damage to healthy tissue and off-site toxicity is but one key advantage that PDT holds over traditional approaches to systemic cancer chemotherapy in particular. The localized and immediate burst of relatively nonspecific, primitive cytotoxic agents mediated by the PSs leads to rapid cellular destruction and less chance for the development of intrinsic or acquired resistance,[1] and this is particularly important when considering prolonged treatment or the widespread use of targeted antibiotics.

Despite the promotion of PDT and PDI as powerful tools for medicine, these strategies have not reached their full potential owing to the poor chemical characteristics of clinically approved PSs. These organic, porphyrin-based systems employ triplet excited states to photogenerate cytotoxic singlet oxygen ($^1O_2$) and other reactive oxygen species (ROS) upon light activation. This requirement for oxygen along with a tendency to photobleach, poor aqueous solubility, and prolonged retention in tissues has spurred an interest in photoactive metal complexes as alternatives.[2] In contrast to the organic PSs, metal complexes possess a variety of excited state configurations that can be accessed through rational changes to their inherently modular scaffolds: metal-to-ligand charge transfer (MLCT), metal-centered (MC), ligand-centered (LC) or intraligand (IL), intraligand charge transfer (ILCT), metal-to-metal charge transfer (MMCT), and combinations thereof. Such states can sensitize $^1O_2$ (Type II), participate in oxygen-dependent and oxygen-independent Type I electron transfer processes, form covalent adducts, and release biologically active molecules.[3] Judicious integration of functional PDT ligands and coligands is capable of producing a breadth of photophysics and photochemistry with wavelengths of light, from ultraviolet (UV) to near-infrared (NIR).

Special Issue: Current Topics in Photochemistry

Received: May 2, 2014
Revised: June 9, 2014
Published: June 13, 2014

Low-lying ^{3}IL excited states with slow decay kinetics are of immense interest because they can prolong the lifetimes of Ru(II) coordination complexes through equilibration with MLCT states or by acting as distinct states.[4] Wrighton and coworkers demonstrated in the 1970s that organic chromophores could be tethered to metal complexes to extend their excited state lifetimes,[5−8] and Ford and Rogers later applied this concept to Ru(II) complexes in order to lengthen their typical 1 μs lifetimes 10-fold.[9] Lifetimes in excess of 150 μs[4,10,11] have been reported for pure ^{3}IL states, and recently we achieved lifetimes as long as 240 μs with 5-(pyren-1-ylethynyl)-1,10-phenanthroline (5-EPP, Chart 1).[12] We found that these lifetimes could be tuned from 22 to 270 μs in fluid solution by changing the attachment point between the pyrenyethnyl group and the coordinating [1,10]-phenanthroline (phen) ligand in complexes of the type $[Ru(LL)_2(EPP)]^{2+}$ or the number of EPP ligands. Interestingly, all of these structural isomers produced a very potent PDT effect in cancer cells, including a metastatic melanoma model.

Chart 1. Molecular Structures of Common Ancillary Ligands and Functional Ligands of Interest

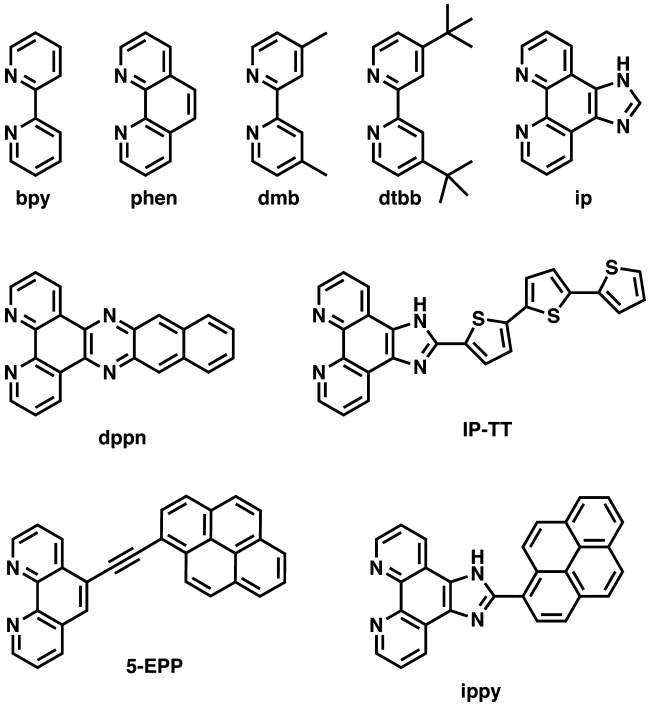

We have since shown that this potency in photodynamic applications is a general phenomenon associated with complexes derived from ligands that impart low-lying ^{3}IL states and suitably long excited state lifetimes, notably benzo[*i*]dipyrido[3,2-*a*:2′,3′-*c*]phenazine (dppn)[13] and 2-(2′,2″:5″,2‴-terthiophene)-imidazo[4,5-*f*][1,10] phenanthroline (IP−TT).[14] Moreover, these nominally blue/green-absorbing PSs can be activated in the PDT window despite no discernible absorption of light at these wavelengths, which underscores the efficiency of such highly photosensitizing excited states.[13] This activity appears to hold for both contiguously fused π-systems and true tethered dyads, whereby the π-expansive organic chromophore is attached to a coordinating ligand such as 2,2′-bipyridine (bpy) or phen via a coannular bond or linker. Herein we outline the photophysical properties and photodynamic potency of another type of metal−organic dyad with a low-lying ^{3}IL state.

Transition metal complexes of 1*H*-imidazo[4,5-*f*][1,10]-phenanthroline (ip) have been well-studied as DNA probes,[15] with a desire to identify frameworks that exhibit site-specific or pH-defined interactions with certain nucleobase sequences. The 2-position of the imidazole fragment of the ip ligand serves as a convenient handle for introducing DNA-interacting substituents, and numerous systems derived from 2-aryl substitution have been described.[16−21] When the aryl group is a π-expansive unit such as pyrene, low-lying ^{3}IL states can substantially alter the excited state dynamics that are otherwise governed primarily by the interaction between the lowest energy ^{3}MLCT state and a higher lying ^{3}MC state in Ru(II) polypyridyl constructs.[22,23] A series of four Ru(II) dyads that incorporate 2-(1-pyrenyl)-1*H*-imidazo[4,5-*f*][1,10]-phenanthroline (ippy) as the functional PDT ligand were prepared in order to expand the repertoire of Ru(II) complexes that exhibit unusual potency due to low-lying ^{3}IL excited states (Chart 2). To our knowledge their in vitro PDT and PDI have not been explored.

2. EXPERIMENTAL SECTION

2.1. Materials. 2,2′-Bipyridine (bpy), 4,4′-dimethyl-2,2′-bipyridine (dmb), 4,4′-di-*t*-butyl-2,2′-bipyridine (dtbb), 1,10-phenanthroline (phen), 1,10-phenanthroline-5,6-dione, pyrene-1-carbaldehyde, and $RuCl_3 \cdot xH_2O$ were purchased from Sigma-Alrich and used without further purification. $[Ru(bpy)_2Cl_2] \cdot 2H_2O$ and precursor complexes of other coligands $[Ru(LL)_2Cl_2]$ were prepared by established procedures.[24] The purified complexes were isolated as PF_6^- salts and subsequently subjected to anion metathesis on Amberlite IRA-410 with methanol to yield the more water-soluble Cl^- salts for biological experiments.

Characterized fetal bovine serum (FBS) and Iscove's Modified Dulbecco's Medium (IMDM) supplemented with 4 mM L-glutamine were purchased from Fisher Scientific, and human promyelocytic leukemia cells (HL-60) were procured from the American Type Culture Collection. Prior to use, FBS was divided into 40 mL aliquots that were heat inactivated (30 min, 55 °C) and subsequently stored at −20 °C. *Streptococcus mutans* (ATCC 25175) was purchased from the American Type Culture Collection. Plasmid pUC19 DNA was purchased from New England BioLabs and transformed using NovaBlue Singles Competent Cells purchased from Novagen. Transformed pUC19 was purified using the QIAprep Spin Miniprep Kit purchased from Qiagen (yield ≈ 62 μg of plasmid DNA per 20 mL culture). Water for biological experiments was deionized to a resistivity of 18 MΩ·cm using a Barnstead filtration system. Calf-thymus DNA (activated type XV) was purchased from Sigma and reconstituted with 5 mM Tris buffer supplemented with 50 mM NaCl (pH 7.4) overnight at room temperature following sonication. The concentration of the resulting DNA solution was calculated from its absorbance at 260 nm using ε_{260} = 6600 M^{-1} cm^{-1} per nucleobase of calf thymus DNA.[25]

2.2. Synthesis and Characterization. The ippy ligand and final Ru(II) complexes **1**−**4** were synthesized according to modified literature protocols using microwave irradiation at 180 °C for 10 min and characterized by thin layer chromatography (TLC) and ^{1}H nuclear magnetic resonance (NMR). The previously unreported complexes **3** and **4** were further characterized by mass spectrometry. The preparation of the ippy ligand[26,27] and compounds **1**[26] and **2**[27] have been

Chart 2. Molecular Structures of Ruthenium(II) Complexes 1−4

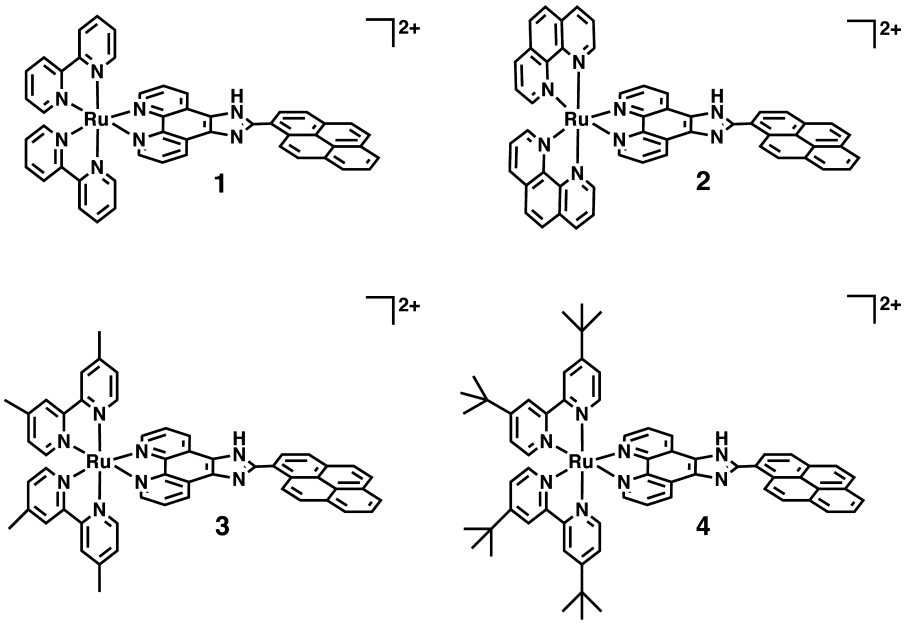

reported. ^{1}H NMR spectra were collected on PF_6^- salts in CD_3CN, and electrospray ionization ESI (+ve) mass spectra were run on PF_6^- or Cl^- salts in acetonitrile or methanol, respectively.

To our knowledge complexes **3** and **4** have not been reported. These compounds were prepared by combining $Ru(4,4'\text{-dmb})_2Cl_2$ or $Ru(dtbb)_2Cl_2$ (0.10 mmol) and ippy (0.10 mmol) in a microwave pressure vessel containing argon-purged ethylene glycol (3.0 mL). The mixture was subjected to microwave irradiation at 180 °C for 10 min. The resulting dark red solution was diluted with water and then washed with dichloromethane to remove residual ligand. Saturated KPF_6 was added dropwise (1−2 mL) to the remaining aqueous phase until no more precipitate formed. The product was then extracted into dichloromethane and evaporated under reduced pressure to give a red solid. The crude material was purified on silica, eluting with 7.5% H_2O in MeCN with 0.5% saturated aqueous KNO_3 to give pure product as a mixture of PF_6^- and NO_3^- salts, which was subsequently dissolved in H_2O with sonication. The desired PF_6^- salt was precipitated with saturated KPF_6, extracted into dichloromethane, and concentrated under reduced pressure to give the product as a pure salt, which was converted to the water-soluble chloride salt on Amberlite IRA-410 anion exchange resin.

$[Ru(bpy)_2(ippy)](PF_6)_2$ (**1**). 85%. $R_f \approx 0.51$ in 7.5% H_2O−MeCN, 2.5% saturated $KNO_{3(aq)}$. ^{1}H NMR (300 MHz, CD_3CN): δ 9.55 (d, J = 9.4 Hz, 1H; d), 9.13 (d, J = 8.3 Hz, 2H; c), 8.66 (d, J = 8.2 Hz, 1H, e), 8.60−8.49 (m, 6H; 3,3′,a), 8.39 (m, J = 8.4 Hz, 4H; 6,6′), 8.29 (d, 1H; (i), 8.18−8.02 (m, 6H; 4,b,j,h), 7.92−7.83 (m, 4H; 4′,k,g), 7.66 (d, J = 5.6 Hz, 2H; l,f), 7.49 (t, J = 6.6 Hz, 2H; 5), 7.27 (t, J = 6.6 Hz, 2H; 5′).

$[Ru(phen)_2(ippy)](PF_6)_2$ (**2**). 52%. $R_f \approx 0.63$ in 7.5% H_2O−MeCN, 2.5% saturated $KNO_{3(aq)}$. ^{1}H NMR (300 MHz, CD_3CN): δ 9.42 (d, J = 10.4 Hz, 1H; c), 9.19 (d, J = 16.0 Hz, 2H; a), 8.80 (d, J = 8.3 Hz, 4H; 2,9), 8.69 (s, 1H; c), 8.58 (d, J = 8.2 Hz, 1H; e), 8.45−8.38 (m, 7H; 5,6,h,d,i), 8.35 (s, 2H; 4), 8.18 (d, J = 5.2 Hz, 2H; 7,j), 8.14−8.09 (m, 2H; g,f), 8.04 (d, J = 4.6 Hz, 2H; l,k), 7.88−7.76 (m, 6H; 3,8,b).

$[Ru(dmb)_2(ippy)](PF_6)_2$ (**3**). 42%. $R_f \approx 0.68$ in 7.5% H_2O−MeCN, 2.5% saturated $KNO_{3(aq)}$. ^{1}H NMR (300 MHz, CD_3CN): δ 9.87 (d, J = 9.3 Hz, 2H ; c), 9.14 (d, J = 8.1 Hz, 2H; a), 8.46−8.31 (m, 8H; ; 3,3′,6,6′), 8.24 (d, J = 5.4 Hz, 1H; d), 8.16 (m, J = 7.4 Hz, 2H; g,k), 8.04 (d, J = 5.3 Hz, 2H; e,i), 7.81 (dd, J = 8.3, 5.2 Hz, 2H; b), 7.71 (d, J = 5.7 Hz, 2H; j,h), 7.48 (d, J = 5.8 Hz, 2H; l,f), 7.31 (d, J = 5.8 Hz, 2H; 5), 7.09 (d, J = 5.8 Hz, 2H; 5′), 2.60 (s, 6H; 4-CH_3), 2.50 (s, 6H; 4′-CH_3). MS (ESI+) m/z: 1035.3 $[M - PF_6]^+$, 445.1 $[M - 2PF_6]^{2+}$. HRMS (ESI+) m/z for $C_{53}H_{40}N_8Ru$: calcd 445.1204, found 445.1199.

$[Ru(dtbb)_2(ippy)](PF_6)_2$ (**4**). 55%. $R_f \approx 0.66$ in 7.5% H_2O−MeCN, 2.5% saturated $KNO_{3(aq)}$. ^{1}H NMR (300 MHz, CD_3CN): δ 9.57 (d, J = 9.4 Hz, 1H; d), 9.09 (d, J = 8.3 Hz, 2H; c), 8.66 (d, J = 8.1 Hz, 1H; e), 8.50 (m, J = 13.3 Hz, 6H; 3,3′), 8.42−8.30 (m, 4H; 6,6′), 8.28 (d, J = 4.8 Hz, 2H; a), 8.17 (d, J = 7.6 Hz, 1H; (i), 8.02 (d, J = 5.2 Hz, 2H; g,k), 7.83 (dd, J = 8.3, 5.3 Hz, 2H; b), 7.72 (d, J = 6.1 Hz, 2H; j,h), 7.55−7.44 (m, 4H; 5,l,f), 7.23 (d, J = 6.7 Hz, 2H; 5′), 1.46 (s, 18H, 4-^{t}butyl), 1.36 (s, 18H; 4′-^{t}butyl). MS (ESI+) m/z: 1203.5 $[M - PF_6]^+$, 529.2 $[M - 2PF_6]^{2+}$. HRMS (ESI+) m/z for $C_{65}H_{64}N_8Ru$: calcd 529.2143, found 529.2140.

Basic photophysical characterization was performed on dilute solutions (5 μM) in spectroscopic-grade MeCN. Oxygen was removed from room temperature samples by sparging a 4 mL solution of PS in a long-neck quartz cuvette (Luzchem SC-10L) with argon at a pressure of 50 ± 10 mmHg for 30 min. Quantum yields of emission (Φ_{em}) were estimated at room temperature according to eq 1 (s refers to sample; r refers to reference) using $[Ru(bpy)_3](PF_6)_2$ as a reference (Φ_{em} = 0.062[22] in deoxygenated MeCN, 0.012[28] in aerated acetonitrile, and 0.38[22] at 77 K in frozen 4:1 v/v ethanol−methanol). Absorption spectra were recorded with a Jasco V-530 spectrophotometer. Steady-state luminescence spectra were measured on a PTI Quantamaster setup equipped with a K170B PMT for measuring ultraviolet and visible emission and a Hamamatsu R5509-42 NIR PMT for measuring near-infrared (NIR) emission (<1400 nm). Short phosphorescence lifetimes (~1 μs) were measured on a PTI LaserStrobe Spectrofluor-

ometer with an R928 stroboscopic detector, pumped by a GL-3300 nitrogen/GL-301 dye laser (2−3 nm fwhm). Long phosphorescence lifetimes (>1 μs) and time-resolved emission spectra were recorded on a PTI Quantamaster setup equipped with a gated detector with a xenon flash lamp as the excitation source. Excited-state lifetimes were extracted from the observed data using PTI Felix32 fitting software. Emission and excitation spectra were corrected for the wavelength-dependence of lamp output and detector response. Singlet oxygen quantum yields (Φ_Δ) were estimated using eq 1 relative to $[Ru(bpy)_3](PF_6)_2$ (Φ_Δ = 0.57 in aerated acetonitrile).[29,30]

$$\Phi_s = \Phi_r\left(\frac{I_s}{A_s}\right)\left(\frac{A_r}{I_r}\right)\left(\frac{\eta_s^2}{\eta_r^2}\right) \quad (1)$$

2.3. DNA Binding by UV−Vis. Optical titrations of PSs with DNA were carried out on a Jasco V-530 absorption spectrophotometer equipped with an ETC-505S/ETC-505T thermoelectric Peltier temperature controller. These titrations were performed in a 1.0 cm × 1.0 cm × 4.5 cm quartz cuvette (3.5 mL) purchased from Hellma Cells fitted with a Teflon-coated magnetic stir bar. The stirring feature on the Peltier controller was used to stir the sample solution throughout the absorption measurement, thereby ensuring that the added CT DNA was mixed into the sample thoroughly.

Optical titrations were carried out on 2 mL solutions of the dyads with increasing amounts of calf thymus DNA (diluted from 5 mM DNA bases stock) to give [DNA bases]/[Ru] between 0.1 and 15. DNA was added in 0.76−10 μL increments to solutions of compound (20 μM) in 5 mM Tris with 50 mM NaCl at pH 7.4. The dilution of metal complex concentration at the end of each titration, although negligible, was accounted for in the binding constant analyses. The DNA binding constant (K_b) was obtained from fits of the titration data to eq 2,[31,32] where $b = 1 + K_bC_t + K_b[DNA]_t/2s$, C_t and $[DNA]_t$ represent the total dyad and DNA concentrations, respectively, s is the binding site size,[33] and ε_a, ε_f, and ε_b represent the molar extinction coefficients of the apparent, free, and bound metal complexes, respectively. ε_f was calculated at absorption maxima >300 nm for **1**−**4** before the addition of DNA, and ε_a was determined at these wavelengths after each addition of DNA. The value of ε_b was determined from the plateau of the DNA titration, where the addition of DNA did not result in any further decrease in the absorption signal. Detailed fits of the titration data were obtained using Kaleidagraph (Synergy Software, Version 4.3).

$$\frac{\varepsilon_a - \varepsilon_f}{\varepsilon_b - \varepsilon_f} = \frac{b - (b^2 - 2K_b^2C_t[DNA]_t/s)^{1/2}}{2K_bC_t} \quad (2)$$

2.4. DNA Photocleavage Assays. DNA photocleavage experiments were performed according to a general plasmid DNA gel mobility shift assay[34−36] with 20 μL total sample volumes in 0.5 mL microfuge tubes. Transformed pUC19 plasmid (129 ng in 1.6 μL, >95% Form I) was added to 10 μL of 10 mM Tris-HCl buffer supplemented with 100 mM NaCl (pH 7.5). Serial dilutions of the Ru(II) compounds were prepared in ddH_2O and added in 5 μL aliquots to the appropriate tubes to yield final PS concentrations in the range of 1−10 μM, and deionized H_2O was added to bring the final assay volumes to 20 μL. Sample tubes were kept at 37 °C in the dark or irradiated. PDT treatments employed visible light (7.8 mW cm^{-2}, 14 J cm^{-2}) delivered for 30 min inside a photoreactor (Luzchem LZC-4X photoreactor equipped with 14 LES-Vis-01 bulbs). After PDT treatment, all samples (dark and light) were quenched by the addition of 4 μL gel loading buffer (0.025% bromophenol blue and 40% glycerol), loaded onto 1% agarose gels cast with 1× TAE (40 mM Tris-acetate and 1 mM EDTA, pH 8.2) containing ethidium bromide (0.75 μg mL^{-1}) and electrophoresed for 30 min at 80 V cm^{-1} in 1× TAE. The bands were visualized with UV-transillumination (UVP transilluminator) and processed using the Gel Doc-It Imaging system (UVP) and the GNU Image Maniupulation Program (GIMP).

2.5. HL-60 Cell Culture. HL-60 human promyelocytic leukemia cells (ATCC CCL-240) were cultured at 37 °C under 5% CO_2 in RPMI 1640 (Mediatech Media MT-10−040-CV) supplemented with 20% FBS (PAA Laboratories, A15-701) and were passaged 3−4 times per week according to standard aseptic procedures. Cultures were started at 200,000 cells mL^{-1} in 25 cm^2 tissue culture flasks and were subcultured when growth reached 800,000 cells mL^{-1} to avoid senescence associated with prolonged high cell density. Complete media was prepared in 200 mL portions as needed by combining RPMI 1640 (160 mL) and FBS (40 mL, prealiquoted and heat inactivated), in a 250 mL Millipore vacuum stericup (0.22 μm) and filtering.

2.6. HL-60 Cell Viability Assays. Experiments were performed in triplicate in 96-well microtiter plates (Corning Costar, Acton, MA), where outer wells along the periphery contained 200 μL pH 7.4 phosphate buffered saline (PBS) with 2.68 mM potassium chloride, 1.47 mM potassium phosphate monobasic, 0.137 M sodium chloride, and 8.10 mM sodium phosphate dibasic to minimize evaporation from sample wells. HL-60 cells growing in log phase (approximately 8 × 10^5 cells) were transferred in 50 μL aliquots to inner wells containing warm culture medium (25 μL) and placed in a 37 °C, 5% CO_2 water-jacketed incubator (Thermo Electron Corp., Forma Series II, Model 3110, HEPA Class 100) for 1 h to equilibrate. Ruthenium compounds were serially diluted with PBS and prewarmed before 25 μL aliquots of the appropriate dilutions were added to the cells and incubated at 37 °C under 5% CO_2 for drug-to-light intervals of 1 or 16 h. Untreated microplates were maintained in a dark incubator, while PDT-treated microplates were irradiated with visible light (400−700 nm, 27.8 mW cm^{-2}) using a 190 W BenQ MS510 overhead projector or with red light (625 nm, 28.7 mW cm^{-2}) from an LED array (Fenol Farm, Inc.). The irradiation time was 1 h to yield light doses of approximately ∼100 J cm^{-2}. Both dark and PDT-treated microplates were incubated for another 48 h at which point prewarmed, 10 μL aliquots of Alamar Blue reagent (Life Technologies DAL 1025) were added to all sample wells and allowed to incubate for 15−16 h at 37 °C under 5% CO_2. Cell viability was determined based on the ability of the Alamar Blue redox indicator to be metabolically converted to a fluorescent dye by live cells. Fluorescence was quantified with a Cytofluor 4000 fluorescence microplate reader with the excitation filter set at 530 ± 25 nm and emission filter set at 620 ± 40 nm. EC_{50} values for cytotoxicity and photocytotoxicity were calculated from sigmoidal fits of the dose response curves using Graph Pad Prism 6.0 according to eq 3, where y_i and y_f are the initial and final fluorescence signal intensities. For cells growing in log phase and of the same passage number, EC_{50} values were reproducible to within ±25% in the submicromolar regime; ±10% below 10 μM; and ±5% above 10 μM.

$$y = y_i + \frac{y_i - y_f}{1 + 10^{(\log EC_{50} - x) \times (\text{Hill slope})}} \quad (3)$$

2.7. *S. mutans* Bacterial Culture. *Streptococcus mutans* stock culture (ATCC 25175, 0.5 mL) was grown on nutrient rich BHI (Oxoid CM225) agar plates overnight in a 37 °C incubator according to the manufacturer's instructions in order to establish growth colonies. To a 15 mL sterile centrifuge tube containing 5 mL of 3.8% (w/v) BHI (aqueous), 2−3 individual bacterial colonies were added, vortexed well to mix, and incubated overnight. The tube was then centrifuged, the supernatant was slowly removed, and the bacterial pellet was reconstituted with a sterile 70% glycerol solution. The tubes were stored in a −80 °C freezer. Experimental cultures were maintained each week by making fresh overnight growths from the frozen stock of *S.mutans* by transferring 50 μL of frozen (thawed) stock to 5 mL of fresh BHI media and vortexed to mix. Cell concentrations were determined using a spectrophotometer set at 600 nm in 1 mL cuvettes, where an O.D. of 0.3 represents approximately 10^8 cells mL^{-1}.[37]

2.8. *S. mutans* Bacterial Survival Assays. Photodynamic inactivation (PDI) of *S. mutans* growing as planktonic cultures[38] and as biofilm[39] was probed by a modification of published procedures. Dark and light experiments were each performed in duplicate in 96-well microtiter plates (Corning Costar, Acton, MA), where outer wells along the periphery contained 200 μL of pH 7.4 phosphate buffered saline (PBS) (no Ca^{2+} or Mg^{2+}). On day one, BHI broth (100 μL) was added to cell-free control wells, while 90 μL of BHI was added to cells-only control wells and to sample wells. The plates were then warmed to 37 °C, and 10 μL of stock bacterial solution (~10^8 CFU mL^{-1}) was added to the control cell wells and to the sample wells. The plates were incubated overnight in a humidified atmosphere at 37 °C to allow for biofilm formation.

2.8.1. Planktonic Assay Plates. On day two, planktonic assay plates were prepared by transferring 200 μL of sterile PBS (no Ca^{2+} or Mg^{2+}) to the outer wells of another set of microtiter plates. Cell-free control wells received 100 μL of PBS, while control cell wells and sample wells received 25 μL of PBS. The plates were then warmed to 37 °C, and 50 μL of planktonic bacterial cells (supernatant) from the biofilm plates was transferred to the control cell wells and the sample wells on the planktonic assay plates. Dilutions of aqueous stock solutions of PSs **1**−**4** were prepared in PBS such that 25 μL additions to the planktonic assay wells yielded PS concentrations between 1 pM and 100 μM. The addition of prewarmed PS aliquots to the sample wells (and prewarmed PBS to the control cell wells) gave final assay volumes of 100 μL. The plates were treated analogous to the HL-60 cell viability assay plates thereafter, except that a 37 °C incubator was used rather than 37 °C with 5% CO_2. The PS-to-light interval was 1 h, and the data analysis was performed as described for the HL-60 cell viability assays.

2.8.2. Biofilm Assay Plates. On day two, any residual supernatant containing planktonic bacteria was removed from the biofilms on the biofilm plates. The BHI broth in the cell-free control wells was also removed for consistency. The biofilms were washed twice with 200 μL of PBS, and this wash was also done on cell-free wells to ensure that all wells, including controls, were treated identically. Next, 100 μL of PBS was added to the cell-free wells, and 75 μL of PBS was added to the biofilm control wells and sample wells. The plates were incubated overnight at 37 °C to re-establish biofilm formation (in case there was any loss of integrity in the wash steps, which can happen if the films are thin and delicate at this stage). Prewarmed PS dilutions in PBS (25 μL) were added to the sample wells (25 μL of prewarmed PBS was added to each biofilm control well) to yield final assay volumes of 100 μL. The dark and light biofilm assay plates were treated and analyzed as described for the planktonic assay plates.

2.9. Aqueous Spectroscopy. The UV−vis spectra of compounds **1**−**4** were recorded at room temperature in air-equilibrated water (except for **4**, which was dissolved in water with 5% DMSO) in a quartz cell with 1 cm path length using a Jasco V-670 spectrophotometer.

Emission spectra of **1**−**4** upon the addition of DNA in buffered solution (5 mM Tris buffer, 50 mM NaCl) were recorded with a Jasco FP-6200 spectrofluorometer at room temperature in an ultra micro quartz cell with 1 cm path length and a volume of 100 μL by using a 5.7 μM solution of **1**−**4**. Various amounts of 1.54 mM calf thymus DNA (CT-DNA) solution were added, and the DNA:MC ratio was adjusted to a maximum value of 70:1 in increments of 5:1. For each ratio a separate solution was prepared. Before each emission measurement, the DNA−MC mixture was allowed to incubate for 20 min.

Resonance Raman (RR) spectra were recorded with a conventional 90° scattering arrangement. For excitation within the range of the MLCT absorption band, an argon ion laser was used (Model Coherent Innova 300C, λ = 458, 476, and 488 nm). A rotating cell was utilized to avoid photodegradation of the sample.[40] The scattered light was focused onto the entrance slit of an Acton SpectraPro 2750 spectrometer and was detected by a liquid nitrogen-cooled CCD camera (Princeton Instruments). The concentration of the complex solution in the RR measurements was optimized to obtain the maximum signal-to-noise ratio and was in the range of 10^{-4} M.

To determine the excited-state lifetimes, nanosecond transient absorption spectra were recorded. Nanosecond pump-pulses were delivered by a Continuum Surelite OPO Plus pumped by a Continuum Surelite Nd:YAG laser (pulse duration 5 ns; pulse-to-pulse repetition rate 10 Hz), and a 75 W xenon arc lamp served as the probe light. Spherical concave mirrors were used to focus the probe light at the sample and to refocus the light on the entrance slit of a monochromator (Acton, Princeton Instruments). The probe light was detected by a Hamamatsu R928 photomultiplier tube mounted on a five-stage base at the monochromator exit slit, and the signal was processed by a commercially available detection system (Pascher Instruments AB). The sample was excited by pump pulses centered at 410 nm. To test for the sensitivity of the long-lived excited states to the presence of oxygen,[41,42] the sample was prepared with and without oxygen using the freeze−pump−thaw method.

The sample integrity was ensured by measuring absorption spectra before and after each spectroscopic experiment. No alterations of the absorption spectra indicative of sample degradation during the measurement were observed.

2.10. Confocal Microscopy. In a laminar flow hood under aseptic conditions, sterile glass-bottom Petri dishes (MatTek) were coated with poly-L-lysine (Ted Pella) by applying 200 μL to the dish, swirling to mix, covering, and allowing to sit. After 1 h the poly-L-lysine was poured off, and the dish was washed 3× with sterile phosphate buffered saline (PBS) containing 2.68 mM potassium chloride, 1.47 mM potassium phosphate monobasic, 0.137 M sodium chloride, and 8.10 mM sodium

phosphate dibasic, pH 7.4. The dishes were left to dry, uncovered, for approximately 15 min. HL-60 human promyelocytic leukemia cells (ATCC CCL-240) were transferred in aliquots of 500 μL (approximately 100,000 cells) to the poly-L-lysine-coated glass bottom Petri dishes and placed in a 37 °C, 5% CO_2 water-jacketed incubator (Thermo Electron Corp., Forma Series II, Model 3110, HEPA Class 100) for 15 min to allow cells to adhere to the coated dishes. Then, 500 μL of warmed 200 μM solutions of PS made in sterile PBS was added to duplicate dishes (for dark and light treatments) and returned to the incubator for 30 min. After the pre-PDT incubation period, one dish was irradiated with white light for 15 min with a 600 W Bell and Howell model 301 transparency projector (power density = 41.7 mW cm^{-2}, total light dose ≈ 7.5 J cm^{-2}). The dark dish was covered with foil and placed in a drawer for the same amount of time. Cells were imaged at 15 min and at 4 h post-treatment using a Zeiss LSM 510 laser scanning confocal microscope (Carl Zeiss Inc.) with a 40× oil objective lens. Excitation was delivered at 458/488 nm from an argon−krypton laser, and signals were acquired through a long pass filter of 560 nm. Pinhole diameters for the all treatments were 60 μm. The images were collected and analyzed using the Zeiss LSM Image Browser Version 4.2.0.121 (Carl Zeiss Inc.).

3. RESULTS AND DISCUSSION

3.1. Synthesis and Characterization. Compounds **1**[26] and **2**[27] have been reported; **1** was previously studied in the context of its remarkable luminescent oxygen sensing and **2** for its DNA affinity and photocleavage. We prepared dyads **1**−**4** in a similar manner except that microwave irradiation at 180 °C for 10 min was used to facilitate reaction times. ^{1}H NMR spectra were assigned for the dyads based on the chemical shifts reported for **1** and **2** (Supporting Information), and the structures of **3** and **4** were further confirmed by mass spectrometry. The PF_6^- salts of the dyads were used to study their spectroscopic properties in MeCN, and the corresponding Cl^- salts were employed to study their spectroscopic properties in water and to explore their biological interactions in aqueous buffer.

The UV−vis absorption spectra collected in MeCN for the Ru(II) dyads in this study were a composite of bpy or phen LC (or IL) transitions below 300 nm, ippy LC or pyrene-based transitions near 370 nm, and typical MLCT transitions around 450−460 nm with shorter wavelength shoulders at 420−430 nm (Figure S8, Supporting Information). The extinction coefficients agree with commonly accepted values for ^{1}LC $\pi \rightarrow \pi^*$ and ^{1}MLCT $d\pi \rightarrow \pi^*$ electronic transitions (Table 1).[43−47] Similar spectra were collected in water (Figure 1), but the longest-wavelength MLCT absorption bands underwent 4−19 nm bathochromic shifts (Table 2).

Table 1. Absorption Maxima and Corresponding Extinction Coefficients for Compounds 1−4 Collected in Aerated MeCN

compd	$\lambda_{max\ abs}$ (nm) (log ε)
1	234 (4.86), 282 (5.00), 368 (4.59), 424 (4.29), 456 (4.31)
2	222 (4.98), 260 (5.05), 280 (4.82), 374 (4.61), 422 (4.36), 448 (4.36)
3	234 (4.70), 282 (4.89), 370 (4.46), 428 (4.12), 464 (4.18)
4	230 (4.87), 282 (5.04), 368 (4.62), 430 (4.35), 462 (4.34)

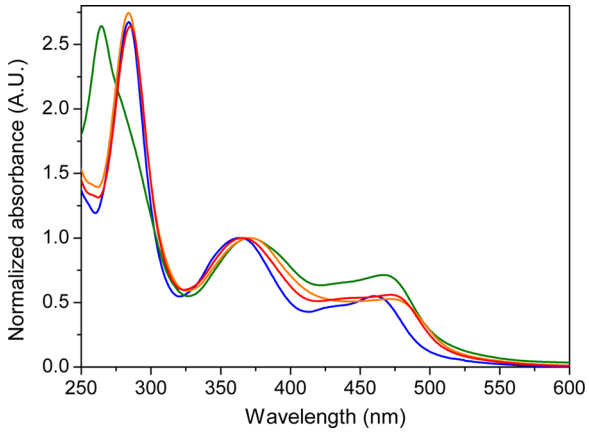

Figure 1. UV−vis absorption spectra of **1** (blue), **2** (green), **3** (orange), and **4** (red) in water. The data are normalized to the maximum value of the low-energy LC band centered near 370 nm.

Table 2. Absorption and Emission Spectroscopic Data for Complexes 1−4

	absorption			emission
compd	λ_{MLCT} (nm)[a]	λ_{MLCT} (nm)[b]	$\Delta\lambda_{MLCT}$ (nm)	λ_{MLCT} (nm)[a]
1	456	460	4	595
2	448	467	19	590
3	464	472	8	611
4	462	471	9	614

[a]Measured in water. [b]Measured in MeCN.

Resonance Raman spectra of **1** in water were recorded with excitation at 458, 476, and 488 nm in order to confirm that the longest wavelength MLCT transition involved ippy rather than another coligand (Figure 2). To identify the vibrational

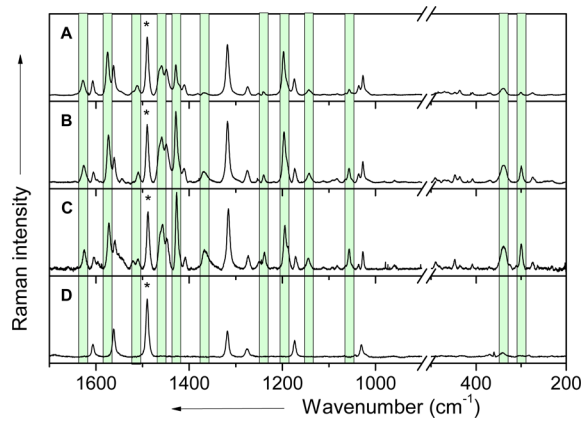

Figure 2. Resonance Raman spectra of **1** in water recorded upon excitation at (A) 458, (B) 476, and (C) 488 nm. (D) Resonance Raman spectrum of $[Ru(bpy)_3]^{2+}$ as a reference with an excitation wavelength of 458 nm. All spectra were normalized to the intensity of the bipyridine band at 1490 cm^{-1} (denoted with an asterisk). The bands that are associated with the ippy ligand are highlighted.

signatures associated with the bpy ligands, the homoleptic complex $[Ru(bpy)_3]^{2+}$ was measured as a reference with an excitation wavelength of 458 nm. By comparison with the spectrum of $[Ru(bpy)_3]^{2+}$, the bands at 300, 1367, 1427, 1457, and 1572 cm^{-1} were assigned to vibrational modes of the ippy ligand. As longer excitation wavelengths were employed, the

overall contribution of the ippy-related modes to the RR spectra increased as would be expected if the lowest-energy MLCT transition were Ru(dπ) → ippy(π*).[48]

Compounds **1**−**4** were weakly emissive (Φ_{em} = 0.13−1.5%) in MeCN (Table 3). This broad, structureless luminescence was centered between 618 and 641 in MeCN, with **2** being the most red-shifted (and **1** being the least). All emission maxima were blue-shifted in water by 20−50 nm, but their relative ordering did not parallel what was observed for MeCN. In fact, the emission maximum of **2** in water was shifted hypsochromically compared to the other compounds (Table 2).[49]

Table 3. Emission Parameters for Compounds 1−4 Collected in Deaerated MeCN

compd	λ_{em} (nm)	τ_{em1} (μs)[a]	τ_{em2} (μs)[b]	Φ_{em} ($\times 10^{-3}$)[c]	Φ_{Δ}[d]
1	618	1.25 (0.15)	83.3 (0.85)	4.2	0.73
2	641	0.78 (0.45)	87.7 (0.55)	1.3	0.83
3	635	1.20 (0.60)	58.1 (0.40)	7.5	0.84
4	635	1.11 (0.51)	46.5 (0.49)	15	∼1

[a]Measured using stroboscopic detection. [b]Measured using a gated detector and constrained in the fit of the stroboscopic biexponential decay. [c]Measured relative to aerated $[Ru(bpy)_3]^{2+}$ (Φ_{em} = 0.012) as the standard. [d]Measured relative to aerated $[Ru(bpy)_3]^{2+}$ (Φ_{Δ} = 0.57) as the standard. Numbers in parentheses are pre-exponential factors for the biexponential fits normalized to 1 for the respective lifetimes. Errors are 10% for lifetime measurements, 20% for Φ_{em} owing to weak emission, and 5% for Φ_{Δ}.

3.2. Photophysical Properties. While the lifetime of dyad **1** was previously reported as a single exponential with τ = 2.5 μs (deaerated MeCN)[26] and considered to be long relative to the usual ^{3}MLCT state lifetimes of Ru(II) polypyridyl complexes (∼0.6−1 μs), we resolved this emission into two components, τ_1 = 1.3 μs and τ_2 = 83 μs (Table 3). The contribution of τ_2 to the overall emission of **1** using stroboscopic methods was minor, but gated collection on a phosphorescence detector enabled precise determination of τ_2, which was subsequently used in a biexponential fit of the stroboscopic data. For complexes **2**−**4**, the same procedure was used to extract τ_1 and τ_2, but in these systems τ_2 was clearly visible using stroboscopic detection. Across the series, τ_1 and τ_2 ranged between 0.78−1.25 and 58−88 μs (deaerated MeCN), respectively, and appear to be a general phenomenon associated with these dyads (Table 3).

The electronic absorption signatures for compounds **1**−**4** were summations of the individual organic and inorganic units, indicating that these dyads are weakly coupled systems with distinct chromophores. When the inorganic-contributed ^{3}MLCT state is in close energetic proximity (∼500 cm^{-1}) to the organic $\pi\pi$* triplet, these two configurations can exist in equilibrium.[50] The $^3\pi\pi$* state of pyrene has been estimated at 16 900 cm^{-1}, or 2.1 eV,[51,52] and 16 400 cm^{-1}, or 2.0 eV, when appended to Ru(II)-coordinating ligands such as bpy or phen.[4] We assume that the energetics of this ^{3}IL state are similar in ippy and coordinated ippy and also isoenergetic with ^{3}MLCT states estimated near 1.9−2.0 eV from the emission maxima of **1**−**4**. However, equilibrated ^{3}MLCT and ^{3}IL states would be expected to decay with a common rate that is a linear combination of the intrinsic deactivation rates for the two states, giving rise to single exponential kinetics.[4] Instead dyads **1**−**4** decay via a double exponential process. Given the small ^{3}MLCT−^{3}IL energy gaps inferred across this series and biphasic kinetics, two possibilities emerge: (1) luminescence occurs from both states, each with a distinct lifetime, or (2) luminescence is from a single state in which τ_1 represents pre-equilibrium relaxation of the emitting state and τ_2 involves decay from the equilibrated mixture via the expected single rate constant. Gated emission measurements could not isolate the second component τ_2 as a distinct spectral profile with ^{3}IL characteristics, and 77 K emission (deaerated 4:1 EtOH−MeOH) led to monoexponential decays between 5 and 10 μs for all four complexes. Therefore, we tentatively ascribe the biexponential process we observe to (2): luminescence from a single emitting state, where τ_1 is pre-equilibrated relaxation from the ^{3}MLCT state and τ_2 involves relaxation of the equilibrated mixtures through the ^{3}MLCT channel.

Biexponential decay kinetics were also observed for the dyads in deaerated water, and the details for compound **1** are described as an example. If the aqueous photophysical profile of dyad **1** mirrors that observed in MeCN, then τ_1 was shortened from 1.3 μs to 650 ns and τ_2 from 83 to 20.3 μs (Figure 3A, red

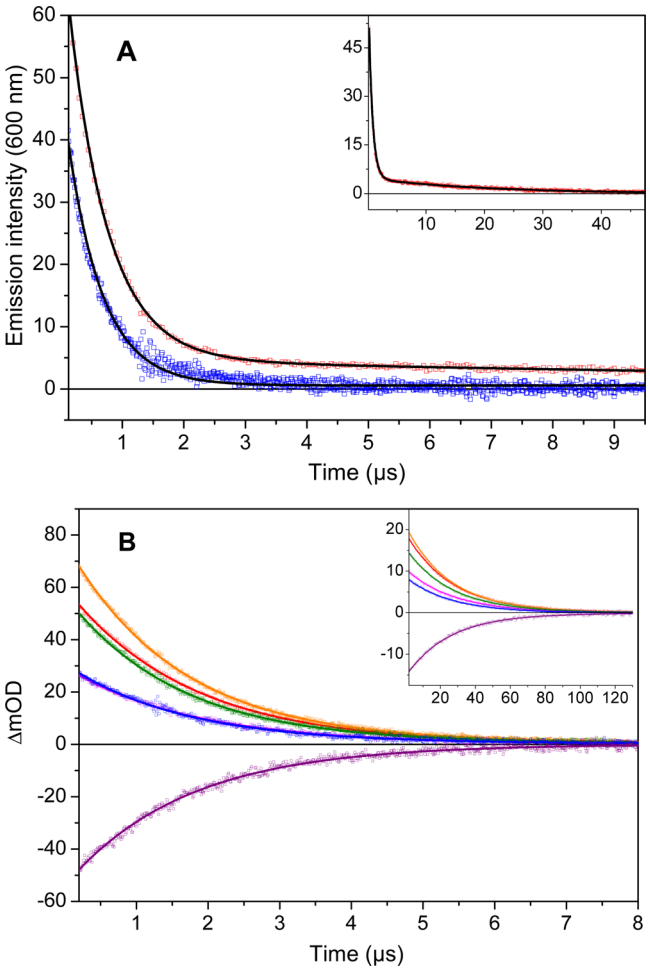

Figure 3. (A) Emission decay kinetics at 600 nm collected with pump pulses centered at 410 nm for oxygen-containing (blue) and oxygen-free (red) **1** in water. Inset displays the complete decay of the oxygen-free species. Symbols represent experimental data, while solid lines refer to the respective mono- or biexponential fitting curves. (B) Transient absorption kinetics recorded at 380 (violet), 450 (blue), 475 (green), 510 (orange), 555 (red), and 650 nm (magenta) for **1** in water (λ_{pump} = 410 nm). Oxygenated kinetics are displayed in the full graph, and oxygen-free kinetics are shown in the inset.

curve), which again suggests close energetic proximity of the lowest-lying ^{3}MLCT state and the pyrene-localized ^{3}IL state with slow equilibration kinetics and efficient ^{3}MLCT decay.[10,44,53] When oxygen was introduced to the environment, τ_2 was quenched entirely and τ_1 (570 ns) was attenuated only slightly (Figure 3A, blue curve). Assignment of τ_1 to pre-equilibrated ^{3}MLCT emission[10,44,53] suggests that the equilibrated mixture (τ_2) plays a more important role in excited state quenching processes by molecular oxygen. Therefore, the high $^1O_2$ quantum yields, 100% for dyad **4** (Table 3), can be attributed to the influence of ^{3}IL states on the excited state trajectory of these systems. Not only are the excited states of these PSs extremely sensitive for luminescent oxygen sensing applications as in the case of **1** (K_{SV} = 0.2393 Torr^{-1}),[26] but also they are poised to act as potent photobiological agents for PDT applications.

The biphasic relaxation kinetics of **1** in water were also probed by transient absorption spectroscopy at different wavelengths with 410 nm excitation (Figure 3B). As expected for dyad systems with strong contributions from weakly coupled pyrenyl units, λ_{probe} = 380 nm gave a negative signal in the TA spectrum, attributed to the ground state bleach due to $^1\pi\pi^*$ pyrenyl absorption. At longer probe wavelengths, positive signals corresponded to ground state recoveries on the μs time scale. In oxygen-free solution, **1** decayed mono-exponentially with a lifetime of 26 μs that coincided with τ_2 extracted from the oxygen-free, aqueous emission experiments. In aerated water, relaxation occurred with a single time constant of 1.6 μs, which was similar to τ_1 measured by emission in deaerated MeCN but slightly longer than that measured by emission in oxygen-free or aerated water. The monoexponential decay (τ_1) in oxygen-containing water was expected, given that τ_2 was completely quenched in the analogous emission experiments, but the absence of the fast component (τ_1) in oxygen-free solution should be considered. If the excited state absorption of the ^{3}MLCT and ^{3}IL configurations are overlapping and the $^3\pi\pi^* \rightarrow n$ transition is sufficiently intense, it is possible that τ_1 is present but cannot be resolved with transient absorption. Regardless, observation of τ_1 and τ_2 in both the aqueous emission and TA experiments combined with biphasic kinetics in at least two solvents via emission measurements argue that low-lying ^{3}IL states drastically influence the excited state dynamics in these dyads. Consequently, the sensitivity that has been documented for these ^{3}IL states toward oxygen and other excited state quenchers[12−14,34] indicates that **1**−**4** will follow suit as potent PSs for PDT.

3.3. DNA Binding. DNA binding of the chloride salts of compounds **1**−**4** to CT DNA was monitored by absorption and emission spectroscopy. The absorption titrations were carried out on 20 μM PS in the presence of increasing amounts of DNA with [DNA bases]/[PS] = 0.1−15. The binding constants calculated (λ > 300 nm) from fits of the binding isotherms to eq 2 ranged from 1.68 × 10^6 to 7.99 × 10^6 M^{-1} ([DNA] in bases), with K_b for **3** and **4** being 4- to 5-fold larger than that calculated for **1** or **2** (Table 4). The reported K_b for **2** is 3.14 × 10^6 M^{-1} ([DNA] in bases),[27] which is very close to our value. By comparison, K_b values for a nonintercalating metal complex such as $[Ru(phen)_3]^{2+}$ and a known intercalator such as $[Ru(phen)_2dppz]^{2+}$ are 1.65 × 10^4 and >10^7 M^{-1} ([DNA] in bases), respectively. While optical titrations alone are not sufficient to classify the mode of PS binding to DNA, the binding constants and site sizes are similar to other known intercalators that stack on the DNA helix,[34,54,55] and pyrenyl units are known to stack with DNA base pairs.[56,57] Therefore, it is reasonable to assign the predominant mode of interaction with DNA as intercalation by the ippy ligand. In the present series, steric bulk on the coligands amplified the strong DNA binding interactions provided by the pyrenyl-containing ippy ligand.

Table 4. DNA Binding Constants and Binding Site Sizes Measured for Compounds 1−4 (20 μM in 5 mM Tris and 50 mM NaCl at pH 7.4) and Calf Thymus DNA ([NP]/[PS] = 0.1-15); Error Limits: K_b,s = ±10%

compd	K_b [10^6 M^{-1}]	s [base pairs]
1	1.68	0.41
2	3.33	0.31
3	7.99	0.36
4	6.55	0.21

As was the case in both MeCN and water, emission from complexes **1**−**4** was also very weak in aqueous buffer. In the presence of DNA, the emission from each complex increased almost 10-fold (Figures 4A and S1−S3, Supporting Information) and reached a plateau at [DNA bp]/[PS] = 30:1 (Figure 4B). This light switch effect is not observed for nonintercalating

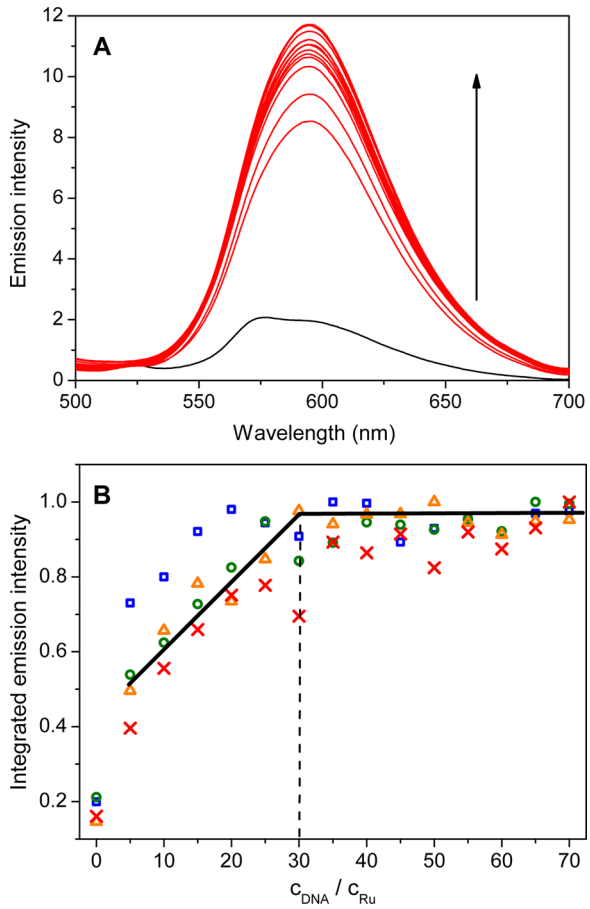

Figure 4. (A) Emission spectra of **1** (5.7 μM) recorded upon excitation at λ_{ex} = 480 nm in the absence (black curve) and presence (red curves) of increasing amounts of CT DNA (28.5−399 μM base pairs) in buffer. (B) Integrated emission intensity of **1** (blue square), **2** (green circle), **3** (orange triangle), and **4** (red cross) for different [DNA]/[PS]. The data were normalized to the maximum emission intensity of each complex.

complexes of the type $[Ru(bpy)_3]^{2+}$ or $[Ru(phen)_3]^{2+}$ that lack solvent-interacting heteroatoms or conformational flexibility but has been documented extensively for $[Ru(bpy)_2dppz]^{2+}$ since its first report in 1990.[58] This light reporting feature of the Ru(II)-ippy dyads, albeit attenuated relative to Ru(II) complexes of dppz, provided a convenient handle for imaging the PSs in live cells and discerning viability. It is not limited to DNA but appears to be a more general molecular light switch mechanism that can be activated in other hydrophobic environments such as lipid membranes and certain proteins. The inability of the imidazole unit to participate in hydrogen bonding interactions and the induced rigidity across the imidazole−pyrenyl coannular bond are key factors that may suppress nonradiative relaxation pathways and enhance emission when the dyads are associated with biological macromolecules.

3.4. Photodynamic Activity. *3.4.1. DNA Photodamage.* Light-responsive agents can damage biomolecules directly or can sensitize the production of reactive intermediates (ROS, RNS, etc.) that, in turn, damage biological macromolecules. This photobiological activity can be readily discerned using plasmid DNA as a probe. The topological integrity of supercoiled, circular DNA (Form I) is extremely sensitive to single- and double-strand breaks (ssb and dsb) as well as nucleobase oxidation, which translates to indirect strand scission under gel electrophoretic conditions (pH 8.5). One ssb is sufficient to cause complete relaxation to nicked, circular DNA (Form II), where no supercoils remain, and as a result, Form II DNA migrates more slowly than Form I when electrophoresed through an agarose gel. Two interstrand ssbs that occur within about 16 base pairs or frank dsbs produce linear DNA (Form III), which migrates between Forms I and II on an agarose gel. Agents that facilitate DNA catenation or condensation produce other noncanonical forms of DNA that are characterized by unique banding and migration patterns. Extremely aggregated DNA, for example, has almost no gel electrophoretic mobility and stays near the loading well (Form IV).

Incubation of plasmid pUC19 DNA (20 μM bases) with PSs **1**−**4** (1−10 μM) followed by exposure to a moderate visible light treatment resulted in almost complete conversion of Form I to Form II DNA in the case of **1**−**3** at PS-to-NP ratios (r_i) of only 0.5 (Figure 5). Compound **4** produced Form II DNA at lower r_i and facilitated aggregation to yield Form IV DNA at higher r_i. In the control treatments, DNA exposed to light only (Lane 2) and DNA exposed to the highest concentration of PS in the dark (Lane 13), no photocleavage was observed. However, the PSs at 10 μM did cause DNA to aggregate in the absence of a light trigger. Faint banding in some lanes can be attributed to PS interference with the fluorescent indicator dye (ethidium bromide) used to image the DNA bands; this interference results from competition for intercalative binding sites, fluorescence quenching, or loss of DNA structural integrity. The strong affinity of these compounds for DNA coupled with their high $^1O_2$ singlet oxygen quantum yields make **1**−**4** potent DNA photocleavers. Moreover, their long-lived triplet excited states result in extreme sensitivity to trace amounts of oxygen and other excited-state quenchers,[26] which could lead to DNA photodamage even at low oxygen tension. Provided that the photoreactivity of these dyads is mediated by reactive intermediates rather than DNA-specific mechanisms, this photodynamic activity is anticipated to extend to other biomolecules determined by subcellular localization. Importantly, activity of this magnitude is well-poised for in vitro PDT in cancer cells and photodynamic inactivation (PDI) of microorganisms.

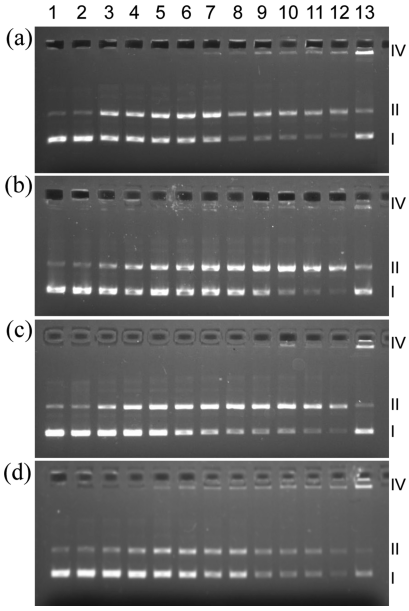

Figure 5. DNA photocleavage of pUC19 plasmid (20 μM bases) dosed with compound **1** (a), **2** (b), **3** (c), or **4** (d) and 14 J cm^{-2} of visible light. Gel mobility shift assays employed 1% agarose gels (0.75 μg mL^{-1} ethidium bromide) electrophoresed in 1× TAE at 8 V cm^{-1} for 30 min. Lane 1, DNA only (−$h\nu$); lane 2, DNA only (+$h\nu$); lane 3, 1.0 μM PS (+$h\nu$); lane 4, 2 μM PS (+$h\nu$); lane 5, 3 μM PS (+$h\nu$); lane 6, 4 μM PS (+$h\nu$); lane 7, 5 μM PS (+$h\nu$); lane 8, 6 μM PS (+$h\nu$); lane 9, 7 μM PS (+$h\nu$); lane 10, 8 μM PS (+$h\nu$); lane 11, 9 μM PS (+$h\nu$); lane 12, 10 μM PS (+$h\nu$); and lane 13, 10 μM PS (−$h\nu$). Forms I, II, and IV DNA refer to supercoiled plasmid, nicked circular plasmid, and aggregated plasmid, respectively.

3.4.2. In Vitro PDT against Human Leukemia Cells. To test the effectiveness of compounds **1**−**4** as PDT agents in cancer cells, the human promyelocytic leukemia (HL-60) cell line was used as a standard model with the Alamar Blue assay for high-throughput quantification of cell viability.[12,13,34,59] At high concentrations of PS, visual cell counts using a hemocytometer were required due to PS interference with the emission of the indicator dye. Briefly, cells were dosed with increasing PS concentration (1 nM to 300 μM), allowed to incubate for a period of time (PS-to-light interval, $t_{h\nu}$), and subjected to either a dark treatment or a light treatment. All cells were then incubated for 48 h, followed by the addition of Alamar Blue and further incubation for 16 h. Total cell−PS incubation times were 65 or 80 h for $t_{h\nu}$ = 1 h and $t_{h\nu}$ = 16 h, respectively. The standard light treatment used was visible light from a projector delivered over 1 h (100 J cm^{-2}). Effectiveness as an in vitro PDT agent was assessed by comparing dark and light cytotoxicities as EC_{50} values (effective concentrations necessary to reduce cell viability to 50%) and their ratio (phototherapeutic index, PI), where PI = EC_{50} (dark)/EC_{50} (light).

In the HL-60 model, $t_{h\nu}$ = 1 h and 100 J cm^{-2} of visible light produces nanomolar light toxicities and PIs >100 from PSs that possess what we call highly photosensitizing excited states (Figure 6 and Table 5). Such potency in Ru(II) complexes is derived most often from pure low-lying ^{3}IL states or ^{3}IL−^{3}MLCT equilibrium mixtures and can lead to PDT in the therapeutic window (600−850 nm) even when molar

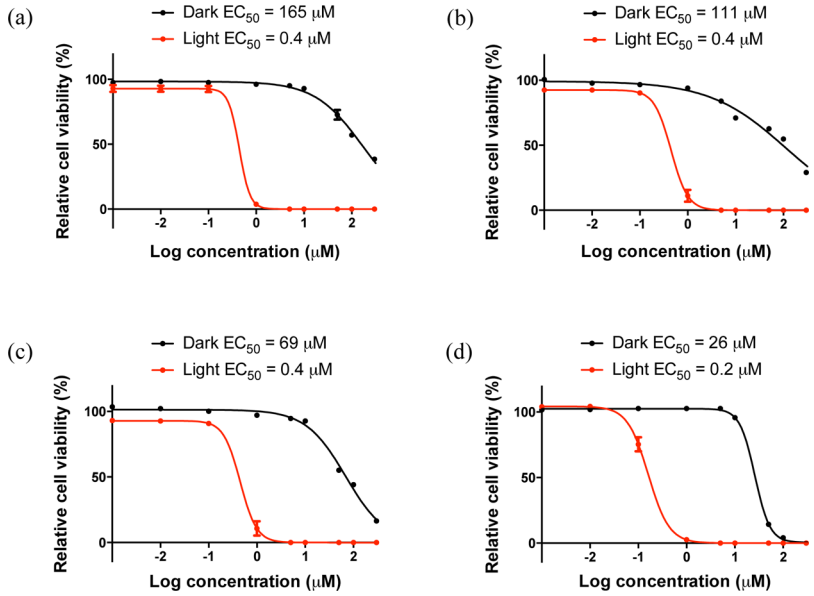

Figure 6. In vitro PDT dose−response curves for complexes **1** (a), **2** (b), **3** (c), and **4** (d) in HL-60 cells. PDT-treated samples were irradiated with 100 J cm^{-2} of white light with a PS-to-light interval of 1 h.

Table 5. EC_{50} Values Calculated from Fits of the in Vitro PDT Dose−Response Curves in Figure 6 and Their Corresponding PI Values

	EC_{50} (μM)		
compd	dark	light	PI
1	165	0.4	413
2	111	0.4	278
3	69	0.4	173
4	26	0.2	130

extinction coefficients for absorption of red light are very low (<100 M^{-1} cm^{-1}).[13,14] The large π-surface area that produces low-lying ^{3}IL states is a convenient platform for DNA binding as well as association with lipophilic membranes and proteins, and the long excited-state lifetimes that characterize these systems provide ample time for generating reactive intermediates or reacting directly with biomolecules. The prolonged lifetimes are particularly sensitive to quenching by molecular oxygen at low oxygen tension,[12,26] which is an attractive feature for retaining activity in hypoxic environments (e.g., cancer cells and tumors).[60,61]

As expected for excited state configurations involving long-lived ^{3}IL states, nanomolar light EC_{50} values (0.2−0.4 μM) were obtained for compounds **1**−**4** (Figure 6) on cells of early passage growing in log phase (n = 4). Dark cytotoxicities increased in the order **1** < **2** < **3** < **4**, with **4** being over six times more toxic than **1** in the dark. Despite the relatively high dark toxicity of **4**, its PI was 130, and the PI values for the other complexes spanned 173−413. Although the absolute numbers for EC_{50} values and PIs varied slightly, this trend held across cells of varying passage number and culture.

Like Ru(II) complexes of dppn[13] and IP−TT[14] containing bpy and dmb coligands, **1**−**3** produced red PDT despite having no appreciable ground state absorption in this regime. However, their light EC_{50} values with 625 nm activation ($t_{h\nu}$ = 1 h, 100 J cm^{-2}) were more than ten times less potent than the corresponding dppn and IP−TT complexes under identical conditions. PI values for red PDT with these dyads ranged from 1.3 to 5.2 and light cytotoxicities were 20−32 μM; with longer PS-to-light intervals ($t_{h\nu}$ = 16 h), the red light toxicities of some of the PSs increased by as much as 5-fold with PIs of almost 10. The order of light EC_{50} values paralleled those for visible light activation except that **3** was slightly more potent than **1** and **2**, and the PI for **4** was marginal owing to a higher dark toxicity relative to the other dyads. The attenuated red PDT in this series could be ascribed to the pre-equilibrium contribution of the ^{3}MLCT to excited state relaxation as well as the existence of an equilibrium mixture rather than pure ^{3}IL states, but this is speculation at this point.

3.5. Cellular Uptake and Localization. HL-60 cells were also used to monitor cellular uptake given that dyads **1**−**4** exhibit the light-switch effect when bound to DNA (Figures 4 and S1−S3, Supporting Information) or sequestered in other hydrophobic environments. The weak luminescence of these PSs in polar media affords the opportunity to image the distribution of these compounds in live cells where they become luminescent. While other techniques (e.g., ICP-MS or AAS) are better suited for quantitative determination of total uptake and subcellular distribution, laser scanning confocal microscopy is an excellent tool for probing cellular uptake and localization in real time (before photobleaching and photodegradation become limiting factors).

The minimal dark cytotoxicity of compounds **1**−**3** at low concentrations of PS (Figure 6a−c) can be rationalized by limited cellular uptake in the absence of a light trigger (Figure 7a). However, when the outer lipid membrane was compromised, as in the case of dead or dying cells, these dyads acted as cell viability indicators (Figure 7a, black arrows). Delivery of a PDT treatment (visible light, 25 J cm^{-2} over 15 min) produced strong red luminescence from the cytosol in a majority of the cell population and some nucleoli (Figure 7b). Apart from the nucleoli (white arrows), very little discernible emission was detected from the nucleus after a 1.25 h total incubation period ($t_{h\nu}$ = 1 h). The onset of photocytotoxicity was rapid so subcellular localization was not tracked as a function of time. Light was necessary for cellular uptake of **1**−**3**, assuming that uptake is directly proportional to intracellular

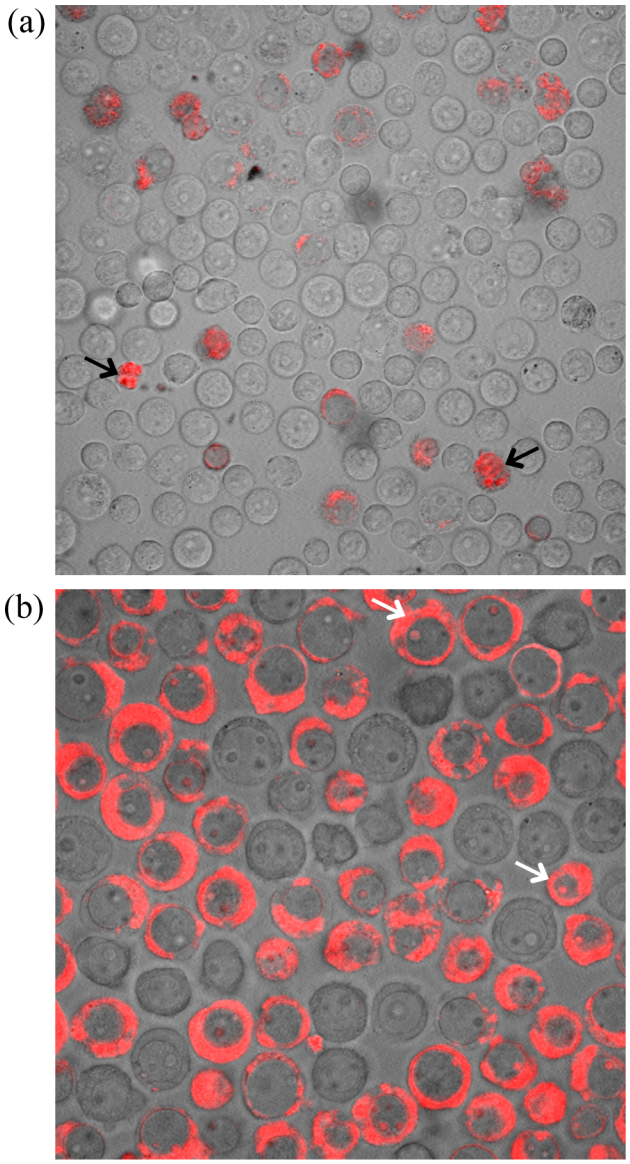

Figure 7. (a) Laser scanning confocal microscopy images of HL-60 cells dosed with **3** (100 μM). (b) HL-60 cells dosed with **3** (100 μM) and incubated for 1 h prior to treatment with visible light (25 J cm^{-2}). Images were collected with λ_{ex} = 458/488 nm and a 560 nm long-pass filter for emission. The diameter of a healthy HL-60 cell is 11−12 μm for scale.

luminescence. Therefore, we infer that initial photoreactivity at the lipid membrane facilitates subsequent influx of the PSs. This orthogonal selectivity serves as an extra layer of protection, preventing very strong DNA intercalators from acting as genotoxins or cytotoxins toward healthy, nonirradiated cells.

The consequence of prolific cellular uptake of a potentially cytotoxic compound was exemplified in the case of dyad **4**, which was cytotoxic to HL-60 cells in the dark at lower concentrations (Figure 6d). Compounds **1** (lowest dark cytotoxicity) and **4** (highest dark cytotoxicity) were compared for their effect on HL-60 cells at relatively high concentration (100 μM) with and without a light treatment (Figure 8). While cellular influx of **1** and ensuing cytotoxicity were acutely dependent on a light treatment (Figure 8a, right panel), compound **4** was taken up by cells regardless of whether light was delivered. Luminescence from both the dark- and light-treated samples was evident in addition to gross morphological changes and clustering. The visual confirmation of a larger PI for **1** follows what might be expected from the incorporation of lipophilic coligands (dtbb) in the architecture of dyad **4**, namely, that increased dark cytotoxicity narrows the therapeutic window for this member of the series. Nevertheless, it should be noted that **4** was twice as potent as the other dyads with visible light activation, giving rise to a visible PI well over 100. Hence, **4** can be delivered to cells in concentrations of up to 10 μM without causing dark cytotoxicity. The major limitation with **4** is the absence of a PDT effect with red light.

3.5.1. PDI of S. mutans. In order to highlight the scope of photodynamic activity for this series, we also probed their abilities to annihilate bacteria through a similar process using visible light activation. We used the oral bacterium *S. mutans* in planktonic culture as a model. The terms photodynamic inactivation (PDI) and photodynamic antimicrobial therapy have become part of the lexicon to describe PDT applied to bacteria. Compounds **1**−**4** invoked PDI against *S. mutans* at nanomolar concentrations, and **1** eliminated more than 75% of the bacterial population at concentrations as low as 10 nM (Figure 9). All of the dyads destroyed almost 100% of the bacteria with little to no dark toxicity at 1 μM. Importantly, this potency was not only maintained against *S. mutans* growing as biofilm, but it was also surpassed with respectable PIs (Figure 10). When microorganisms grow as a community and become irreversibly attached to surfaces (biofilms), their phenotypic properties are notably altered and they become notoriously resistant to antimicrobial agents.[62] These Ru(II) dyads destroyed 100% of the biofilms at 1 μM with almost no dark toxicity. At concentrations of 100 nM, all four of the PSs destroyed at least 70−75% of the biofilms, and **2** was active at 10 nM. This remarkable PDI is currently being developed to treat opportunistic bacteria that cause infections in wounds and colonize implanted surgical devices.

4. CONCLUDING REMARKS

Ru(II) dyads derived from π-expansive organic chromophores represent a general approach to achieving highly photosensitizing states in transition metal complexes that are extremely sensitive to oxygen and other quenchers, and thus offer the opportunity for activity at low oxygen tension, Type I/II photoswitching, and PDT in the therapeutic window. We have demonstrated this phenomenon for Ru(II) coordination complexes containing contiguous π frameworks such as dppn, and for the linked scaffolds EPP and IP−TT, and now ippy. The common factor among these dyads is the existence of a low-lying, long-lived ^{3}IL state that can significantly impact the photophysical dynamics of these systems. In general, the light cytotoxicities against both cancer cells and bacteria are very high, with dark toxicities heavily influenced by the identity of the ancillary ligands. Inclusion of lipophilic dtbb coligands increased the dark cytotoxicity and, consequently, diminished the PI for visible PDT and abrogated the red PDT effect altogether. In a separate report, we will demonstrate that changing the coligand identity can overcome some of these salient challenges and is also a tunable element for improving further the light toxicities and PIs, including high potency in the PDT window. Studies are also underway to document the femtosecond dynamics in these families of Ru(II) dyads with low-lying ^{3}IL states and to explore their collective potential as PSs for multiwavelength PDT in specialized applications.

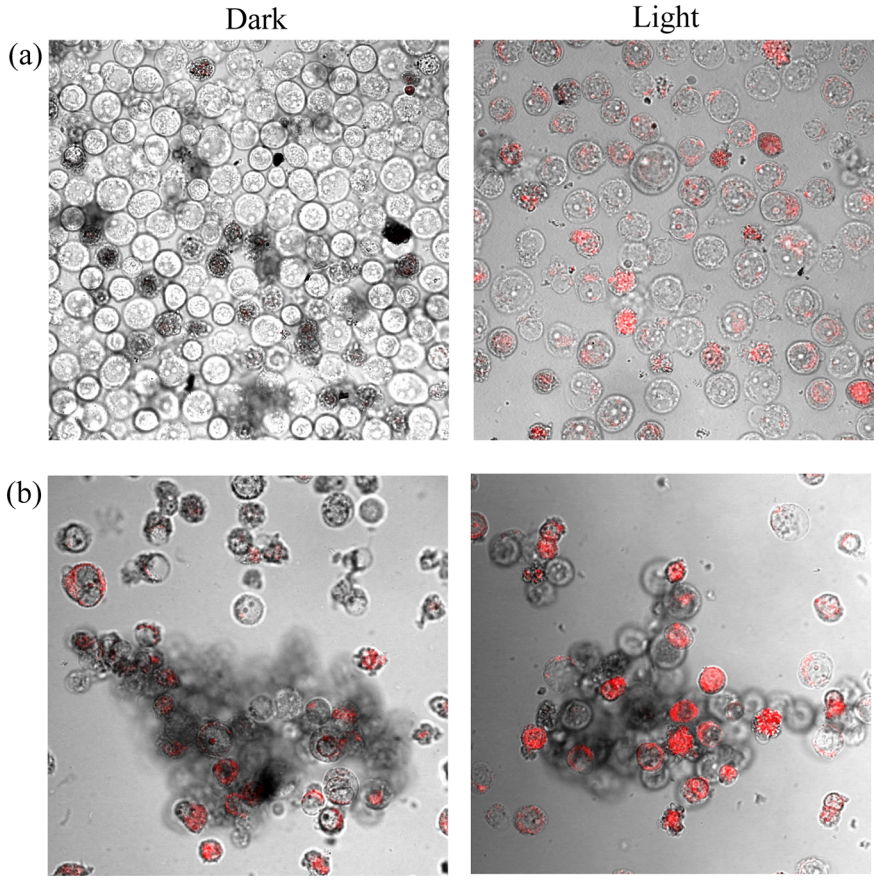

Figure 8. Comparison of HL-60 cells dosed with **1** (a) or **4** (b). HL-60 cells were dosed with PS and either left in the dark (left) or incubated for 1 h prior to a treatment with 38 J cm^{-2} of visible light (right). Images were collected with λ_{ex} = 458/488 nm and a 560 nm long-pass filter for emission. The diameter of a healthy HL-60 cell is 11−12 μm for scale.

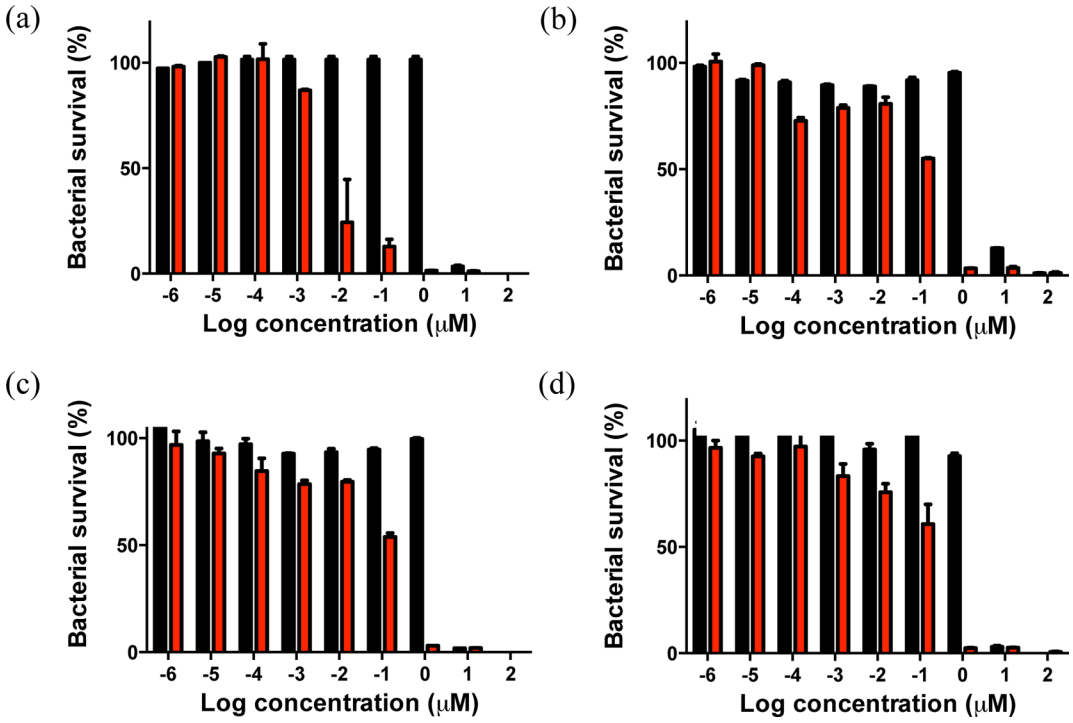

Figure 9. In vitro PDI effect for complexes **1** (a), **2** (b), **3** (c), and **4** (d) against *S. mutans* growing as planktonic cultures. PDI-treated samples (red bars) were irradiated with 100 J cm^{-2} of white light with a PS-to-light interval of 1 h. Black bars represent samples that did not receive a light treatment and indicate baseline antimicrobial activity (if any).

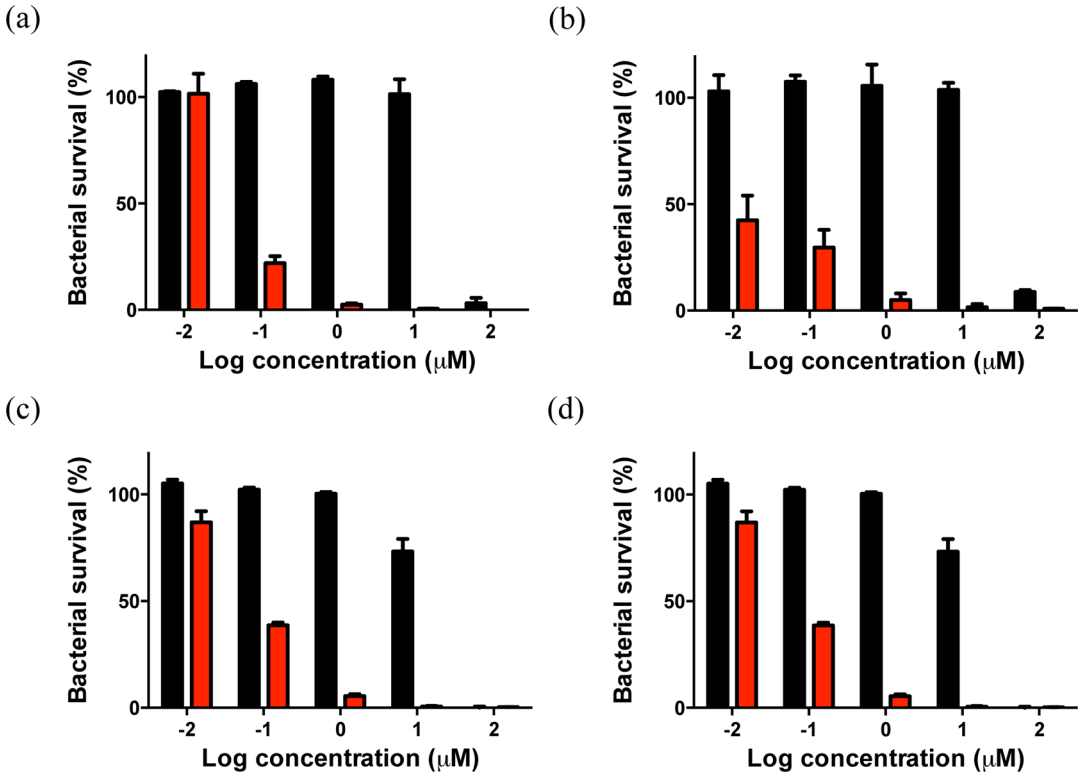

Figure 10. In vitro PDI effect for complexes **1** (a), **2** (b), **3** (c), and **4** (d) against *S. mutans* biofilms. PDI-treated samples (red bars) were irradiated with 100 J cm^{-2} of white light with a PS-to-light interval of 1 h. Black bars represent samples that did not receive a light treatment and indicate baseline antibiofilm activity (if any).

■ ASSOCIATED CONTENT

Supporting Information

Absorption and emission spectra, fluorescence titrations with DNA, and ^{1}H NMR spectra. This material is available free of charge via the Internet at http://pubs.acs.org.

■ AUTHOR INFORMATION

Corresponding Authors

*(S.A.M.) E-mail: sherri.mcfarland@acadiau.ca. Phone: 902-585-1320.

*(B.D.) E-mail: benjamin.dietzek@uni-jena.de. Phone: +49-3641-948360.

Notes

The authors declare no competing financial interest.

■ ACKNOWLEDGMENTS

S.A.M., M.S., M.P., T.S., G.S., H.Y., S.M., and E.S. thank the Natural Sciences and Engineering Research Council of Canada, the Canadian Foundation for Innovation, and the Nova Scotia Research and Innovation Trust for financial support of this work; Prof. Todd Smith for use of his cell and tissue culture facility; and Mr. Haixin Xu and the Acadia Centre for Microstructural Analysis (ACMA) for use of the laser scanning confocal microscope. B.D. and C.R. thank Fonds der Chemischen Industrie and Landesgraduiertenstipendium for funding.

■ REFERENCES

(1) Soukos, N. S.; Goodson, J. M. Photodynamic therapy in the control of oral biofilms. *Periodontology 2000* **2011**, *55*, 143−166.

(2) Farrer, N. J.; Salassa, L.; Sadler, P. J. Photoactivated chemotherapy (PACT): the potential of excited-state d-block metals in medicine. *Dalton Trans.* **2009**, 10690−10701.

(3) Glazer, E. C. Light-activated metal complexes that covalently modify DNA. *Isr. J. Chem.* **2013**, *53*, 391−400.

(4) McClenaghan, N. D.; Leydet, Y.; Maubert, B.; Indelli, M. T.; Campagna, S. Excited-state equilibration: a process leading to long-lived metal-to-ligand charge transfer luminescence in supramolecular systems. *Coord. Chem. Rev.* **2005**, *249*, 1336−1350.

(5) Wrighton, M. S.; Morse, D. L.; Pdungsap, L. Intraligand lowest excited states in tricarbonylhalobis(styrylpyridine)rhenium(I) complexes. *J. Am. Chem. Soc.* **1975**, *97*, 2073−2079.

(6) Giordano, P. J.; Fredericks, S. M.; Wrighton, M. S.; Morse, D. L. Simultaneous multiple emissions from fac-XRe(CO)3(3-benzoylpyridine)2:n-.pi.* intraligand and charge-transfer emission at low temperature. *J. Am. Chem. Soc.* **1978**, *100*, 2257−2259.

(7) Fredericks, S. M.; Luong, J. C.; Wrighton, M. S. Multiple emissions from rhenium(I) complexes: intraligand and charge-transfer emission from substituted metal carbonyl cations. *J. Am. Chem. Soc.* **1979**, *101*, 7415−7417.

(8) Pdungsap, L.; Wrighton, M. S. Photochemistry of cis-tetracarbonylbis(trans-4-styrylpyridine)tungten(0): intraligand photoisomerization from upper excited states. *J. Organomet. Chem.* **1977**, *127*, 337−347.

(9) Ford, W. E.; Rodgers, M. A. J. Reversible triplet-triplet energy transfer within a covalently linked bichromophoric molecule. *J. Phys. Chem.* **1992**, *96*, 2917−2920.

(10) Kozlov, D. V.; Tyson, D. S.; Goze, C.; Ziessel, R.; Castellano, F. N. Room temperature phosphorescence from ruthenium(II) complexes bearing conjugated pyrenylethynylene subunits. *Inorg. Chem.* **2004**, *43*, 6083−6092.

(11) Goze, C.; Kozlov, D. V.; Tyson, D. S.; Ziessel, R.; Castellano, F. N. Synthesis and photophysics of ruthenium(II) complexes with multiple pyrenylethynylene subunits. *New J. Chem.* **2003**, *27*, 1679−1683.

(12) Lincoln, R.; Kohler, L.; Monro, S.; Yin, H.; Stephenson, M.; Zong, R.; Chouai, A.; Dorsey, C.; Hennigar, R.; Thummel, R. P.; McFarland, S. A. Exploitation of long-lived ^{3}IL excited states for metal−organic photodynamic therapy: Verification in a metastatic melanoma model. *J. Am. Chem. Soc.* **2013**, *135*, 17161−17175.
(13) Yin, H.; Stephenson, M.; Gibson, J.; Sampson, E.; Shi, G.; Sainuddin, T.; Monro, S.; McFarland, S. A. In vitro multiwavelength PDT with ^{3}IL states: Teaching old molecules new tricks. *Inorg. Chem.* **2014**, *53*, 4548−4559.
(14) Shi, G.; Monro, S.; Hennigar, R.; Colpitts, J.; Fong, J.; Kasimova, K.; DeCoste, R.; Spencer, C.; Chamberlain, L.; Mandel, A.; et al. Ru(II) dyads derived from *a*-oligothiophenes: A new class of potent and versatile photosensitizers for PDT. *Coord. Chem. Rev.* **2014**, DOI: 10.1016/j.ccr.2014.04.012.
(15) Han, M.-J.; Gao, L.-H.; Wang, K.-Z. Ruthenium(II) complex of 2-(9-anthryl)-1H-imidazo[4,5-f][1,10]phenanthroline: synthesis, spectrophotometric pH titrations and DNA interaction. *New J. Chem.* **2006**, *30*, 208−214.
(16) Xu, H.; Zheng, K.-C.; Chen, Y.; Li, Y.-Z.; Lin, L.-J.; Li, H.; Zhang, P.-X.; Ji, L.-N. Effects of ligand planarity on the interaction of polypyridyl Ru(II) complexes with DNA. *J. Chem. Soc., Dalton Trans.* **2003**, 2260−2268.
(17) Liu, Y.-J.; Guan, X.-Y.; Wei, X.-Y.; He, L.-X.; Mei, W.-J.; Yao, J.-H. Ruthenium(II) complexes containing 2,9-dimethyl-1,10-phenanthroline and 4,4′-dimethyl-2,2′-bipyridine as ancillary ligands: synthesis, characterization and DNA-binding. *Trans. Met. Chem.* **2008**, *33*, 289−294.
(18) Wu, J.-Z.; Ye, B.-H.; Wang, L.; Ji, L.-N.; Zhou, J.-Y.; Li, R.-H.; Zhou, Z.-Y. Bis(2,2′-bipyridine)ruthenium(II) complexes with imidazo[4,5-f][1,10]-phenanthroline or 2-phenylimidazo[4,5-f]-[1,10]phenanthroline. *J. Chem. Soc., Dalton Trans.* **1997**, *24*, 1395−1401.
(19) Liu, Y.-J.; Chao, H.; Yuan, Y.-X.; Yu, H.-J.; Ji, L.-N. Ruthenium(II) mixed-ligand complexes containing 2-(6-methyl-3-chromonyl)imidazo[4,5-f][1,10]-phenanthroline: Synthesis, DNA-binding and photocleavage studies. *Inorg. Chim. Acta* **2006**, *359*, 3807−3814.
(20) Tan, L.-F.; Chao, H.; Li, H.; Liu, Y.-J.; Sun, B.; Wei, W.; Ji, L.-N. Synthesis, characterization, DNA-binding and photocleavage studies of $[Ru(bpy)2(PPIP)]^{2+}$ and $[Ru(phen)2(PPIP)]^{2+}$. *J. Inorg. Biochem.* **2005**, *99*, 513−520.
(21) Fan, S.-H.; Zhang, A.-G.; Ju, C.-C.; Gao, L.-H.; Wang, K.-Z. A triphenylamine-grafted imidazo[4,5-f][1,10]phenanthroline ruthenium(II) complex: acid-base and photoelectric properties. *Inorg. Chem.* **2010**, *49*, 3752−3763.
(22) Juris, A.; Balzani, V.; Barigelletti, F.; Campagna, S.; Belser, P.; von Zelewsky, A. Ru(II) polypyridine complexes: photophysics, photochemistry, eletrochemistry, and chemiluminescence. *Coord. Chem. Rev.* **1988**, *84*, 85−277.
(23) Harriman, A.; Khatyr, A.; Ziessel, R. Extending the luminescence lifetime of ruthenium(II) poly(pyridine) complexes in solution at ambient temperature. *Dalton Trans.* **2003**, 2061−2068.
(24) Sullivan, B. P.; Salmon, D. J.; Meyer, T. J. Mixed phosphine 2,2′-bipyridine complexes of ruthenium. *Inorg. Chem.* **1978**, *17*, 3334−3341.
(25) Fornander, L. H.; Frykholm, K.; Reymer, A.; Renodon-Cornière, A.; Takahashi, M.; Nordén, B. Ca^{2+} improves organization of single-stranded DNA bases in human Rad51 filament, explaining stimulatory effect on gene recombination. *Nucleic Acids Res.* **2012**, *40*, 4904−4913.
(26) Ji, S.; Wu, W.; Wu, W.; Guo, H.; Yang, Q.; Wang, Q.; Zhang, X.; Wu, Y.; Zhao, J. Synthesis of polypyridyl ruthenium complexes with 2-(1-aryl)-1H-imidazo[4,5-f]-1,10-phenanthroline ligand and its application for luminescent oxygen sensing. *Front. Chem. China* **2010**, *5*, 193−199.
(27) Mariappan, M.; Maiya, B. G. Effects of anthracene and pyrene units on the interactions of novel polypyridylruthenium(II) mixed-ligand complexes with DNA. *Eur. J. Inorg. Chem.* **2005**, *2005*, 2164−2173.
(28) Foxon, S. P.; Metcalfe, C.; Adams, H.; Webb, M.; Thomas, J. A. Electrochemical and photophysical properties of DNA metallo-intercalators containing the ruthenium(II) tris(1-pyrazolyl)methane unit. *Inorg. Chem.* **2007**, *46*, 409−416.
(29) DeRosa, M. C.; Crutchley, R. J. Photosensitized singlet oxygen and its applications. *Coord. Chem. Rev.* **2002**, *233/234*, 351−371.
(30) Abdel-Shafi, A. A.; Beer, P. D.; Mortimer, R. J.; Wilkinson, F. Photosensitized generation of singlet oxygen from ruthenium(II)-substituted benzoaza-crown-bipyridine complexes. *Phys. Chem. Chem. Phys.* **2000**, *2*, 3137−3144.
(31) Carter, M. T.; Rodriguez, M.; Bard, A. J. Voltammetric studies of the interaction of metal chelates with DNA. 2. Tris-chelated complexes of cobalt(III) and iron(II) with 1,10-phenanthroline and 2,2′-bipyridine. *J. Am. Chem. Soc.* **1989**, *111*, 8901−8911.
(32) Kalsbeck, W. A.; Thorp, H. H. Determining binding constants of metal complexes to DNA by quenching of the emission of $Pt_2(pop)_4^{-4}$ (pop = $P_2O_5H_2^{-2}$). *J. Am. Chem. Soc.* **1993**, *115*, 7146−7151.
(33) McGhee, J. D.; von Hippel, P. H. Theoretical aspects of DNA-protein interactions: co-operative and non-co-operative binding of large ligands to a one-dimensional homogeneous lattice. *J. Mol. Biol.* **1974**, *86*, 469−489.
(34) Monro, S.; Scott, J.; Chouai, A.; Lincoln, R.; Zong, R.; Thummel, R. P.; McFarland, S. A. Photobiological activity of Ru(II) dyads based on (pyren-1-yl)ethynyl derivatives of 1,10-phenanthroline. *Inorg. Chem.* **2010**, *49*, 2889−2900.
(35) Croke, D. T.; Perrouault, L.; Sari, M. A.; Battioni, J. P.; Mansuy, D.; Helene, C.; Le Doan, J. Structure−activity relationships for DNA photocleavage by cationic porphyrins. *J. Photochem. Photobiol.* **1993**, *18*, 41−50.
(36) Praseuth, D.; Gaudemer, A.; Verlhac, J. B.; Kraljic, I.; Sissoeff, I.; Guille, E. Photocleavage of DNA in the presence of synthetic water-soluble porphyrins. *Photochem. Photobiol.* **1986**, *44*, 717−724.
(37) Murray, P. R.; Baron, E. J.; Jorgensen, J. H.; Pfaller, M. A.; Yolken, R. H., Eds. *Manual of Clinical Microbiology*, 9th ed; ASM Press: Washington, D.C., 2007.
(38) Araújo, N. C.; Fontana, C. R.; Bagnato, V. S.; Gerbi, M. E. M. Photodynamic antimicrobial therapy of curcumin in biofilms and carious dentine. *Lasers Med. Sci.* **2014**, *29*, 629−635.
(39) Lee, Y.-H.; Park, H.-W.; Lee, J.-H.; Seo, H.-W.; Lee, S.-Y. The photodynamic therapy on *Streptococcus mutans* biofilms using erythrosine and dental halogen curing unit. *Int. J. Oral Sci.* **2012**, *4*, 196−201.
(40) Kiefer, W. Raman difference spectroscopy with the rotating cell. *Appl. Spectrosc.* **1973**, *27*, 253−257.
(41) Ollino, M.; Cherry, W. R. Quenching of photosubstitution in ruthenium polypyridine complexes. *Inorg. Chem.* **1985**, *24*, 1417−1418.
(42) Hartmann, P.; Leiner, M. J. P.; Lippitsch, M. E. Luminescence quenching behavior of an oxygen sensor based on a Ru(II) complex dissolved in polystyrene. *Anal. Chem.* **1995**, *67*, 88−93.
(43) Zhen, Q. X.; Ye, B. H.; Zhang, Q. L.; Liu, J. G.; Li, H.; Ji, L. N.; Wang, L. Synthesis, characterization and the effect of ligand planarity of $[Ru(bpy)_2L]^{2+}$ on DNA binding affinity. *J. Inorg. Biochem.* **1999**, *76*, 47−53.
(44) Tyson, D. S.; Bialecki, J.; Castellano, F. N. Ruthenium(II) complex with a notably long excited state lifetime. *Chem. Commun.* **2000**, 2355−2356.
(45) Deng, H.; Cai, J.; Xu, H.; Zhang, H.; Ji, L.-N. Ruthenium(II) complexes containing asymmetric ligands: synthesis, characterization, crystal structure and DNA-binding. *Dalton Trans.* **2003**, 325−330.
(46) Campagna, S.; Puntoriero, F.; Nastasi, F.; Bergamini, G.; Balzani, V. Photochemistry and Photophysics of Coordination Compounds: Ruthenium. In *Photochemistry and Photophysics of Coordination Compounds I*; Balzani, V., Campagna, S., Eds.; Topics in Current Chemistry 280; Springer: Berlin, Germany, 2007.
(47) Zou, X.-H.; Ye, B.-H.; Li, H.; Liu, J.-G.; Xiong, Y.; Ji, L.-N. Mono- and bi-nuclear ruthenium(II) complexes containing a new asymmetric ligand 3-(pyrazin-2-yl)-as-triazino[5,6-f]1,10-phenanthro-

line: synthesis, characterization and DNA-binding properties. *J. Chem. Soc., Dalton Trans.* **1999**, 1423−1428.
(48) Wächtler, M.; Guthmuller, J.; González, L.; Dietzek, B. Analysis and characterization of coordination compounds by resonance Raman spectroscopy. *Coord. Chem. Rev.* **2012**, *256*, 1479−1508.
(49) Bouskila, A.; Amouyal, E.; Verchère-Béaur, C.; Sasaki, I.; Gaudemer, A. Mononuclear and binuclear ruthenium(II) heteroleptic complexes based on 1,10-phenanthroline ligands. Part II: Spectroscopic and photophysical study in the presence of DNA. *J. Photochem. Photobiol. B, Biol.* **2004**, *76*, 69−83.
(50) Simon, J. A.; Curry, S. L.; Schmehl, R. H.; Schatz, T. R.; Piotrowiak, P.; Jin, X.; Thummel, R. P. Intramolecular electronic energy transfer in ruthenium(II) diimine donor/pyrene acceptor complexes linked by a single C−C bond. *J. Am. Chem. Soc.* **1997**, *119*, 11012−11022.
(51) McClure, D. S. Selection rules for singlet-triplet perturbations in polyatomic molecules. *J. Chem. Phys.* **1949**, *17*, 665−666.
(52) Perez-Prieto, J.; Perez, L. P.; González-Béjar, M.; Miranda, M. A.; Stiriba, S.-E. Pyrene-benzoylthiophene bichromophores as selective triplet photosensitizers. *Chem. Commun.* **2005**, 5569−5571.
(53) Tyson, D. S.; Castellano, F. N. Intramolecular singlet and triplet energy transfer in a ruthenium(II) diimine complex containing multiple pyrenyl chromophores. *J. Phys. Chem. A* **1999**, *103*, 10955−10960.
(54) Nair, R. B.; Teng, E. S.; Kirkland, S. L.; Murphy, C. J. Synthesis and DNA-binding properties of $[Ru(NH_3)_4dppz]^{2+}$. *Inorg. Chem.* **1998**, *37*, 139−141.
(55) Haq, I.; Lincoln, P.; Suh, D.; Norden, B.; Chowdhry, B. Z.; Chaires, J. B. Interaction of delta- and lambda-$[Ru(phen)_2DPPZ]^{2+}$ with DNA: a calorimetric and equilibrium binding study. *J. Am. Chem. Soc.* **1995**, *117*, 4788−4796.
(56) Avirah, R. R.; Schuster, G. B. Fluorescence quenching by intercalation of a pyrene group tethered to an N4-modified cytosine in duplex DNA. *Photochem. Photobiol.* **2013**, *89*, 332−335.
(57) Li, L.; Lu, J.; Xu, C.; Li, H.; Yang, X. Studies on the interaction mechanism of pyrene derivatives with human tumor-related DNA. *Molecules* **2012**, *17*, 14159−14173.
(58) Friedman, A. E.; Chambron, J. C.; Sauvage, J. P.; Turro, N. J.; Barton, J. K. A molecular light switch for DNA: $Ru(bpy)_2(dppz)^{2+}$. *J. Am. Chem. Soc.* **1990**, *112*, 4960−4962.
(59) Howerton, B. S.; Heidary, D. K.; Glazer, E. C. Strained ruthenium complexes are potent light-activated anticancer agents. *J. Am. Chem. Soc.* **2012**, *134*, 8324−8327.
(60) Wilson, W. R.; Hay, M. P. Targeting hypoxia in cancer therapy. *Nat. Rev. Cancer* **2011**, *11*, 393−410.
(61) Vaupel, P.; Mayer, A. Hypoxia in cancer: significance and impact on clinical outcome. *Cancer Metastasis Rev.* **2007**, *26*, 225−239.
(62) Hoyle, B. D.; Williams, L. J.; Costerton, J. W. Production of mucoid exopolysaccharide during development of *Pseudomonas aeruginosa* biofilms. *Infect. Immun.* **1993**, *61*, 777−780.